LSPR Sensor Chip Fabricated Based on Au Nanoparticles: Effect of Graphene Oxide and Reduced Graphene Oxide

Zohreh Ayareh
University of Kashan
Mehrdad Moradi (m.moradi@kashanu.ac.ir)
University of Kashan https://orcid.org/0000-0003-3971-840X

Research Article

Keywords: Localized surface plasmon resonance, Au nanoparticles, Self-assembly monolayer, Plasmonic, Reduced graphene oxide, Raman spectroscopy

Posted Date: January 4th, 2022

DOI: https://doi.org/10.21203/rs.3.rs-1096719/v1

Abstract

Nanoparticles of noble metals are well known to display unique optical properties due to the localized surface plasmon resonance (LSPR) phenomenon, making them applicable for use as transducers in various LSPR sensor configurations. In order to develop a sensor chip, Au nanoparticles (AuNPs) were decorated onto a transparent glass substrate in the form of a uniform, high-density single layer using a self-assembly monolayer (SAM) process. The glass substrate surface was initially modified with amine functional groups using different concentrations of (3-Aminopropyl) triethoxysilane (APTES), followed by its optimization to reach a uniform monolayer of AuNPs. The optimized substrate was subsequently prepared by functionalization with APTES, while also being immersed into colloidal AuNPs. A uniform layer of Graphene oxide (GO) and reduced graphene oxide (rGO) sheets were coated on the AuNPs thin films using the dip-coating technique. The AuNPs/GO and rGO hybrid films were employed along with an appropriate optical set up acting as a smart sensor chip for detection of different concentrations of biomaterials. The optimum LSPR sensor (%0.5 APTES immersed in colloidal AuNPs for 12 h) resulted in a chip with %29 absorption and sharper plasmon peak. This appropriate condition remained constant after adding rGO, indicating that Glass/AuNPs/rGO chip will be suitable for sensory applications.

Introduction

Up to now, numerous novel materials with plasmonic properties based on graphene have been discovered, demonstrating very promising application in fields, such as energy storage, sensing, and catalysis [1, 2]. The electrical conductivity, high refractive index, and large surface area of graphene materials attract widespread studies in the field of sensing [3]. The graphene-based sensor exhibits excellent performances such as label-free, and real-time detection manner for the detection of biomolecules, biomarkers, and gas sensing [4, 5]. Graphene oxide is one derivative of graphene which has a dynasty of oxygen-containing groups such as hydroxyl, epoxy, and carboxyl groups. Graphene oxide has been widely utilized as a biosensor material owing to its high electrochemical and chemical activity. Meanwhile, the π–π conjugated networks are broken with these oxidized groups [6]. The GO can be changed to the rGO by removing oxygen-containing groups which presents different properties in certain respects. For example, the hydrophobic rGO tends to aggregation that cause to change its shape and the specific area, although the oxygen-containing groups increase the hydrophilicity so it makes GO more stable greatly in water solution [7]. The well-organized reduction of GO and restoration of π–π conjugated network of structure have provided advantages in electronics and optics fields [8]. In general, the sensors are arranged by depositing the GO or rGO suspension and other functional components such as novel metal nanoparticles on the substrate [9].

Plasmonic nanostructures have unique optical properties that can be represented by the optical cross-section and appropriate wide range of applications in biotechnology [10-12]. Au nanoparticles (AuNPs) have been used in the field of catalysis, optical sensor [13, 14], surface-enhanced Raman spectroscopy (SERS) [15-17], and biological molecule detection based on their optical properties, electrical properties, and various extinction constants [18]. One well-known optical aspect of AuNPs is the localized surface

plasmon resonance, resulting from the interaction of the incident electromagnetic wave with plasmonic nanoparticles which causes a collective oscillation of conduction electrons [19-22]. The wavelength and intensity of LSPR peak in extinction spectra are highly dependent on geometry, dimension in nanoscale, and the dielectric environment surrounding the nanoparticles [23, 24]. The appropriate method emphasized the deposition of graphene oxide and reduced graphene oxide onto the AuNPs LSPR sensor via metal-carbon bonding with a significantly uniform surface and suitable for binding biomolecules [25, 26]. The detection principle of the LSPR sensor chip is the measurement of the change in the refractive index of environment surrounding the plasmonic nanoparticles, as result can enhance the near-field intensity [27].

This beneficial characteristic allows monitoring of surface states and analysis of intermolecular interactions. Self-assembly monolayers are molecular layer and it has an appropriate performance which is widely used for the spontaneous arrangement of nanoparticles on the surface of the substrate. Self-assembly monolayer has been fabricated with coupling agents such as thiol-terminated, amine-terminated, alkyl-terminated, and phenyl-terminated silanes which coupling agents attach on various substrates through their terminal groups and adsorb metal nanoparticles on the surface of the substrate [28]. Among coupling agents, APTES is the popular coupling agent that has been used for surface functionalization. The salinization process takes place with three hydrolysable groups APTES which attach to hydroxyl groups on the glass substrate surface, therefore another group is the amine (NH_2) from the amino propyl groups that adsorb metal nanoparticles on the glass substrate [29]. Thus, the functionalization of the substrate with NH_2-terminated on any substrate is exceptionally important for extra surface modification.

In this paper, we thus established a self-assembly monolayer method to deposit of Au nanoparticles on a transparent glass substrate as a single layer, using the functionalization of the substrate with NH_2-terminated with 0.1, 0.5, 1, 2, and 5% APTES solution. A uniform distribution of GO and rGO were decorated on AuNPs thin film for placing LSPR chip in the optical setup to simply fabricate an LSPR sensor chip. The optimized substrate was subsequently prepared by functionalization with an ideal concentration of %0.5 APTES, while also being immersed into colloidal AuNPs 12 h. The GO and rGO are very promising for connecting to AuNPs, and binding biomolecules.

Experimental

Gold (III) chloride trihydrate ($HAuCl_4 \cdot 3H_2O$, ≥99.9%), Trisodium citrate dihydrate ($Na_3C_6H_5O_7$, ≥99%),), (3-Aminopropyl) triethoxysilane (APTES, ≥97%) hydrochloric acid (HCl, 37%), ethanol (99%), Methanol (MeOH, 98%), Sulfuric acid (H_2SO_4, 98%) were purchased from Merck. Ultrapure deionized water with a resistivity of 18.2 MΩ·cm was used. The suspension of GO sheets of the modified Hummers with 2.7-6.8 μm was purchased from Namago Co. (Tehran, Iran).

Preparation of Citrate- stabilized Au Nanoparticles

Small AuNPs with a mean diameter of 20 nm were synthesized using the Turkevich method [30] as previously reported [31]. Citrate-stabilized Au nanoparticles were prepared in DI water via reduction of HAuCl4 with trisodium citrate. First, a 50 ml aqueous solution of 1 mM $HAuCl_4$ was heated in a beaker to boil. 5 ml of 0.5 mM trisodium citrate solution was added to the $HAuCl_4$ solution and homogenized by gentle stirring. The mixed solution was then heated for an additional 10 min under vigorous stirring. The colour of the solution immediately changed from pale yellow to red, indicating the formation of AuNPs. The reduction of Au ions and capping of resulting nanoparticles both occurred by citrate ions. Finally, the heating was stopped, and the solution of Au nanoparticles was stirred and kept in an ice bath to reach room temperature.

Synthesis of Graphene Oxide Derivatives

There are several ways to reduce GO, including chemical, thermal, hydrothermal, and electrochemical techniques, and chemical methods were used for the reduction of GO and change to rGO [32]. The surface composition in the method of chemically reduced graphene oxides is due to the use of different masses of hydrazine hydrate, sodium borohydride (NaBH4), and this surface composition affect the electron transfer properties [33].

Chemical Reduced GO

Initially, 20 mg/ml of GO suspension in DI water was sonicated for 1h to disperse the suspension. The chemical reaction was performed at 90°C. 0.16 g of $NaBH_4$ was added to the above mixture under continuous stirring. The reaction ended after 48 hours. Finally, the product was washed with DI water until the pH reached neutral and dried in an oven at 65°C [34].

Chip fabrication and Optimization of APTES Concentration

The LSPR chip was fabricated in three steps: hydroxylation of the glass substrate (-OH), salinization of the glass substrate (-NH_2), and attachment of colloidal gold nanoparticles on the glass surface. In the first step, for hydroxylation of the microscope substrate, the glass slides were cut into 7 x 1 cm^2 pieces and cleaned by immersion in freshly prepared 1: 1 MeOH: HCl solution for 30 min, after that immersed in H_2SO_4 for 30 min, followed by rinsing in distilled water and ethanol in an ultrasonic bath, and drying under a stream of N_2. After cleaning, for salinization process, the hydroxyl-functionalized slides were immersed in 0.1, 0.5, 1, 2, and 5% APTES solution in ethanol for 1 h, rinsed with ethanol, and dried with N_2 gas.

In the third step, AuNPs immobilization was achieved by immersing the silanized slides in a colloidal citrate-stabilized AuNPs at various times. By immersion in the colloidal gold nanoparticle solution for 1 and 12 hours, two types of LSPR sensor chips were prepared, and entitled type 1 and type 2, respectively. The glass substrate was then rinsed with water to remove the unbinding AuNPs. A uniform layer of GO and rGO sheets was dip-coated on the AuNPs thin films. At this step, the AuNPs thin films were first immersed in a colloidal solution of GO or rGO for 1 min and drawn upward at a constant rate of 187.5 mm min^{-1}.

Characterization

The LSPR chip sensor includes citrate-stabilized AuNPs immobilized on a glass substrate modified with the organic adhesion layer. The morphology of Au nanoparticles and thin films were visualized by a field emission scanning electron microscope (FESEM) to study the uniformity of the AuNPs monolayer (TESCAN-MIRA3). The UV-Vis spectrum was measured for plasmon absorption analysis (Spectronix Ar 2015). XRD pattern was registered by employing an X-ray diffractogram (Philips) with copper K_a irradiation (λ = 15.4 nm). FT-IR spectrum was measured by the Shimadzu Varian 4300 spectrophotometer in the range of 400–4000 cm^{-1}. Raman spectra were recorded using Lab Ram HR Raman microscope (Horiba) with 50×/0.50NA objective, and a source excitation was 532 nm of green laser.

Results And Discussion

Morphological study

Figure1 shows that the colloidal AuNPs are close to spherical Au nanoparticles with citrate stabilized. After assembly of AuNPs monolayer on the substrate, annealing at temperatures close to Tg (the glass transition temperature (Tg) is the temperature at which the molecular structure shows molecular mobility) of the AuNPs thin films (557°C) results in significant enhancement of the adhesion between the AuNPs and the substrate. Therefore, LSPR sensor chips were annealed at 550°C at a rate of 5°C/min and stayed at this temperature for 4 h. The FESEM image illustrates the size distribution of 10-15 nm nanoparticles (Fig. 2). After self-assembly of AuNPs on a substrate and then annealing, the AuNPs were deposited most uniformly and densely because of aggregation of nanoparticles, the size distribution increased to about 15-20 nm.

Optical Properties and Characterization of GNPs

Figure 3 reveals the XRD pattern of metallic Au nanoparticles on the glass substrate. All diffraction peaks corresponding to face-cantered cubic (fcc) (111), (200), (220), and (311) crystalline planes were well-matched with the JCPDS No. 03-065-8601 of Au. The XRD pattern of Au with the background of glass pattern confirm the distance between Au nanoparticles on the surface. The extinction spectrum of LSPR sensor chips before and after annealing was characterized by UV-Vis spectroscopy and shown in Fig. 4. The UV–Vis spectrum of colloidal AuNPs exhibits a plasmon resonance peak at 522 nm. Annealing of AuNPs thin films leads to an enhancement in the extinction intensity and 10 nm LSPR red-shift. As the nanoparticle size increases, not only does the adsorption rate increase but also the position and width of the LSPR shift.

LSPR sensor chips were performed to optimize the immobilization of amine functional groups on the glass substrate with different concentrations of APTES, which attends as a linking molecule between the glass and the AuNPs. The self-assembly takes place through electrostatic interaction between the positively charged amine group and negatively charged AuNPs.

Figures 5 and 6 depict the surface plasmon peak changes of the LSPR sensor chip to determine the optimal APTES concentration and optimal immersion time in colloidal AuNPs. As shown in Fig. 5, increasing the APTES concentration not only enhances the extinction intensity of the LSPR sensor chip but also an LSPR red-shift exists. However, this treatment has not been followed in Fig. 6. Based on the results shown in Table 1, conditions of 0.5% APTES and 12 h immersion in AuNPs were selected as the optimal condition for the LSPR sensor chip. Because this chip demonstrates the highest extinction intensity and sharp plasmon peak, these features make the sensor chip highly sensitive.

Table 1
The extinction wavelength and intensity of LSPR sensor chip (according to Figs. 5 and 6)

	1 h immersion in colloidal AuNPs					12 h immersion in colloidal AuNPs				
APTES (1 h)	0.1%	0.5%	1%	2%	5%	0.1%	0.5%	1%	2%	5%
Wavelength (nm)	530	535	534	533	543	533	537	534	537	539
Intensity of Extinction (a.b.)	0.175	0.226	0.216	0.199	0.25	0.241	0.295	0.261	0.262	0.271

Due to the synergistic effects, metal/graphene nanostructure hybrids exhibit advanced performance compared to NPs and graphene derivatives taken independently. Hence, attempts have been focused on the decoration of GO/rGO surfaces with AuNPs, which have applications in various fields such as sensors, catalysts, and SERS.

Figure 7 shows the FTIR spectra of GO and rGO in which the GO spectrum contains the absorption bands corresponding to –OH stretch at 3428 cm^{-1}, the C=O carbonyl stretching vibrations at 1602 cm^{-1}, the C-OH stretching at 1384 cm^{-1}, and the epoxy C–O stretching at 1014 cm^{-1}. The spectrum of rGO shows peaks at 3428 cm^{-1}, corresponding to –OH stretch, while the bands of carboxyl, epoxy, and carbonyl were removed after the reduction [35, 36].

Based on the results, the AuNPs thin film for depositing GO and rGO was selected with 0.5% APTES and 12 h immersion in colloidal AuNPs as the optimal condition for the LSPR sensor chip. The GO and rGO layers were used due to their inherent properties of binding the biomolecules and increasing the interaction light with structure [37, 38]. The morphology of LSPR chips of AuNPs/GO and AuNPs/rGO was observed using SEM. As shown in Fig. 8, the GO sheets were recognized in the SEM image. Similarly, the SEM images of AuNPs/GO and AuNPs/rGO are presented in which the uniform distribution of paper-like GO and rGO sheets on AuNPs thin film is visible.

According to Fig. 9, all absorption peaks associated with the GO and rGO sheets are in the visible rang of 400-900 nm, which is the wavelength range of AuNPs LSPR [39]. Detection of the local index of refraction using UV-Visible spectrum corresponding to sharp plasmon peaks for high sensitivity. In this case, LSPR

sensor chip of AuNPs/rGO have sharp plasmon peaks rather than other chips, and redshift confirms the binding of AuNPs and rGO.

Figure 10 shows the Raman spectra of the AuNPs/GO and the AuNPs/rGO films displaying the G band (1593 cm^{-1}) for vibration mode in-plane of sp^2 carbon domains and D band (1347 cm^{-1}) associated with structural defects indicating the reduction in the size of sp^2 domains and increasing of out-plane of sp^3 domains. The I_D/I_G ratio can be described as the number of defects of GO and rGO in the LSPR sensor chip. For the sensor chip of AuNPs/GO, the value of I_D/I_G is equal to 0.78, while for AuNPs/rGO it increases to 0.81. An increase in I_D/I_G shows that partial reduction has increased structural defects in the GO carbon plane [40]. Significant differences in intensity peak intensities can confirm the widespread coupling of AuNPs with rGO, which increases the light interaction in the advanced surface Raman spectroscopy (SERS) configuration. As a short conclusion, Glass/AuNPs/rGO chip will be suitable for sensory applications compared to Glass/AuNPs/GO chip.

Conclusions

AuNPs thin films were prepared by electrostatic binding of citrate-stabilized NPs on amino silane-terminated glass substrates. The AuNPs thin films have been fabricated with different concentrations of APTES and immersion time in colloidal AuNPs to enhance the sensitivity of the LSPR sensor chip. After annealing of the AuNPs thin films at 550° C, the AuNPs were deposited most uniformly and densely. The extinction of the LSPR sensor chip demonstrated that the best condition in the fabrication of LSPR sensor chip was 0.5% APTES and 12 h immersion in AuNPs. The GO and rGO were found to be very promising for connecting to AuNPs and binding biomolecules, so that AuNPs/GO and AuNPs/rGO nanostructures could be employed as efficient biosensors.

Declarations

Acknowledgements

The authors gratefully acknowledge the financial support of this study from the University of Kashan by Grant No. 1093744/1.

Funding This work was supported by the University of Kashan by Grant No. 1093744/1.

Conflicts of interest/Competing interests The authors declare no competing interests.

Availability of data and material All data that support the findings of this study are available from the corresponding author upon reasonable request.

Code availability Not applicable

Authors' contributions Zohreh Ayareh: Investigation, Visualization, Writing – original draft. Mehrdad Moradi: Supervision, Conceptualization, Resources.

Ethics approval Not applicable

Consent to participate Informed consent was obtained from all individual participants included in the study.

Consent for publication All the authors agree to publish these papers.

References

1. Li M; Tang Z; Leng M; Xue J (2014) Flexible solid state super capacitor based on graphene-based hybrid films. *Adv. Funct. Mater.* 24:7495–7502.
2. Kakaei K, Balavandi A (2016) Synthesis of halogen-doped reduced graphene oxide nanosheets as highly efficient metal free electrocatalyst for oxygen reduction reaction. *J. ColloidInterf. Sci.* 463:46–54.
3. Tiwari J N, Vij V, Kemp K C, Kim K S (2016) Engineered carbon-nanomaterial-based electrochemical sensors for biomolecules. *ACS Nano.* 10:46–80.
4. Wang T, Huang D, Yang Z, Xu S S, He G L, Li X L, Hu N T, Yin G L, He D N, Zhang L Y A (2016) review on graphene-based gas/vapor sensors with unique properties and potential applications. *Nano-Micro Lett.* 8:95–119.
5. Yang Y J, Li W K (2014) Gold nanoparticles/graphene oxide composite for electrochemical sensing of hydroxylamine and hydrogen peroxide. *Fuller. Nanotub. Carbon Nanostruct.* 26:195–204.
6. Zhao J, Pei S, Ren W, Gao L, Cheng H M (2010) Efficient Preparation of Large-Area Graphene Oxide Sheets for Transparent Conductive Films. *ACS Nano. 4*:5245–5252.
7. Stankovich S, Piner R D, Chen X, Wu N, Nguyen S T, Ruoff R S (2006) Stable aqueous dispersions of graphitic nanoplatelets via the reduction of exfoliated graphite oxide in the presence of poly (sodium 4-styrenesulfonate). *J Mater Chem.* 16:155–158.
8. Lin T, Chen I, Liu F, Yang C, Bi H, Xu F, Huang F (2015) Nitrogen doped mesoporous carbon of extraordinary capacitance for electrochemical energy storage. *Science.* 350:1508–1513.
9. Wang D, Li W, Zhang Q, *et al.* (2021) High-Performance Tapered Fiber Surface Plasmon Resonance Sensor Based on the Graphene/Ag/TiO_2 Layer. *Plasmonics* 16:2291–2303.
10. Xu T, Geng Zh (2021) Strategies to improve performances of LSPR biosensing: Structure, materials, and interface modification, *Biosens. Bioelectron.* 174:112850.
11. Li Z, Butun S, Aydin K (2014) Touching Gold Nanoparticle Chain Based Plasmonic Antenna Arrays and Optical Metamaterials. *ACS Photonics.* 1(3):228–234.
12. Baciu C L, Becker J, Janshoff A, Sönnichsen C (2008) Protein–Membrane Interaction Probed by Single Plasmonic Nanoparticles. *Nano Letter.* 8(6):1724-1728.

13. Moradi M, Ayareh Z, Mahmoodi S (2019) Magneto-plasmonic biosensing platform for detection of glucose concentration. *Optik.* 178:765-773.
14. Mahmoodi S, Moradi M (2018) Carbon Nanotube Assisted Enhancement of the Magneto-Optical Kerr Signal in Nickel Thin Films. *J. Electron. Mater.* 47:7069-7074.
15. Kasztelan M, Słoniewska A, Gorzkowski M, Lewera A, Pałys B, Zoladek S (2021) Ammonia modified graphene oxide–Gold nanoparticles composite as a substrate for surface enhanced Raman spectroscopy. *Appl. Surf. Sci.* 554:149060.
16. Santhoshkumar S, Murugan E (2021) Rationally designed SERS AgNPs/GO/g-CN nanohybrids to detect methylene blue and Hg^{2+} ions in aqueous solution; *Appl. Surf. Sci.* 553:149544.
17. Jimenez-Vara P B, Johny J, Novoa-de Leon I C, Guerrero-Bermea C, Garcia-Gutierrez D F, Garcia-Gutierrez D I Chavez-Guerrero L, Sepulveda-Guzman S (2020) Hybrid films of reduced graphene oxide modified with gold nanorods and its study as surface-enhanced Raman spectroscopy platform; *Mater. Lett.* 265:127405.
18. Zohora N, Kumar D, Yazdani M, Rotello V M, Ramanathan R, Bansal V (2017) Rapid Colorimetric Detection of Mercury Using Biosynthesized Gold Nanoparticles. *Colloid Interface Sci.* 532:451-457.
19. Sepúlveda B, Angelomé P C, Lechuga L M, Liz-Marzán L M (2009) LSPR-based nanobiosensors. *Nano Today*. 4:244-251.
20. Esmailzadeh B, Moradi M (2018) Enhancement of Kerr Signal in Co Thin Films Incorporating Ag Nanoparticles Surrounded by TiO_2. *J. Supercond. Nov. Magn*. 31:1483-1488.
21. Guerreiro J R L, Frederiksen M, Bochenkov V E, De Freitas V, Ferreira S M G, Sutherland D. S (2014) Multifunctional biosensor based on localized surface plasmon resonance for monitoring small molecule–protein interaction. *Acs Nano*. *8*(8):7958-7967.
22. Xu T, Geng Z (2020) Strategies to improve performances of LSPR biosensing: Structure, materials, and interface modification. *Biosens. Bioelectron.* 174:112850.
23. Dormeny A A, Sohi P A, Kahrizi M (2020) Design and simulation of a refractive index sensor based on SPR and LSPR using gold nanostructures. *Results Phys.* 16:102869.
24. Taghavi A, Rahbarizadeh F, Abbasian S, *et al.* (2015) Label-Free LSPR Prostate-Specific Antigen Immune-Sensor Based on GLAD-Fabricated Silver Nano-columns. *Plasmonics* 15:753–760.
25. Prabowo B A, Purwidyantri A, Liu B, Lai H C, Liu K C (2021) Gold nanoparticle-assisted plasmonic enhancement for DNA detection on a graphene-based portable surface plasmon resonance sensor. *Nanotechnol.* 32(9):095503.
26. Barghouti M E, Akjouj A, Mir A (2018) Effect of graphene layer on the localized surface plasmon resonance (LSPR) and the sensitivity in periodic nanostructure. *Photo. Nano. Fund. Appl.* 31:107-114.
27. Willets K A, Duyne R P V (2007) Localized surface plasmon resonance spectroscopy and sensing. *Annu. Rev. of Phys. Chem.* 58:267-297.
28. Kyaw H H, Al-Harthi S H, Sellai A, Dutta J (2015) Self-organization of gold nanoparticles on silanated surfaces. *Beilstein J Nanotechnol*. 6:2345-2353.

29. Terracciano M, Rea I, Politi J, De Stefano K (2013) Optical characterization of amino silane-modified silicon dioxide surface for biosensing. *The Eur. Opt. Soc.* 8:13075.
30. Turkevich J, Stevenson P C, Hillier J (1951) A study of the nucleation and growth processes in the synthesis of colloidal gold. *Discussions of the Faraday Society*. 11:55-75.
31. Moradi M, Ayareh Z, Mahmoodi S (2017) Enhancement of magneto-optical Kerr response by LSPR in magneto plasmonic nanostructures for biological sensors. *J. Magn. Magn. Mater.* 444:410-415.
32. Feng J, Ye Y, Xiao M, Wu G, Ke Y (2020) Synthetic routes of the reduced graphene oxide. *Chem. Pap.* 74:3767–3783.
33. Tan S M, Ambrosi A, Chua C K, Pumera M (2014) Electron transfer properties of chemically reduced graphene materials with different oxygen contents. *J. Mater. Chem. A. 2*:10668–10675.
34. Báez D F, Pardo H, Laborda I, Marco J F, Yáñez C, Bollo S (2017) Reduced graphene oxides: influence of the reduction method on the electrocatalytic effect towards nucleic acid oxidation. *Nanomater*. *7*(7):168.
35. Yang Z, Zheng Q, Qiu H, Li J, Yang J (2015) A simple method for the reduction of graphene oxide by sodium borohydride with $CaCl_2$ as a catalyst. *New Carbon Mater*. 30(1):41–47.
36. Goncalves G, Marques P A P, Granadeiro C M, Nogueira H I S, Singh M K, Gracio J (2009) Surface Modification of Graphene Nanosheets with Gold Nanoparticles: The Role of Oxygen Moieties at Graphene Surface on Gold Nucleation and Growth. *Chem. Mater.* 21:4796–4802.
37. Xiong X, Chen Y, Wang H, Hu S, Luo Y, Dong J, Zhu W, Qiu W, Guan H, Lu H, Yu J, Zhang J, Chen Z (2018) Plasmonic Interface Modified with Graphene Oxide Sheets Over layer for Sensitivity Enhancement. *ACS Appl. Mater. & Interfaces.10*(41):34916-34923.
38. Liu X, Zhao Z, Shen T, Qin Y (2019) Graphene/Gold nanoparticle composite-based paper sensor for electrochemical detection of hydrogen peroxide. *Fuller. Nanotub. Carbon Nanostruct.* 27:23-27.
39. Singh L, Zhang R B, Cheng S, Kaushik B K, Kumar S (2019) LSPR based uric acid sensor using graphene oxide and gold nanoparticles functionalized tapered fiber. *Opt. Fiber Technol.* 53:102043.
40. Abdelkader-Fernández V K, Melguizo M, Domingo-García M, López-Garzón F J, Pérez-Mendoza M (2019) Hydrogen cold plasma for the effective reduction of graphene oxide. *Appl. Surf. Sci.* 464:673-681.

Figures

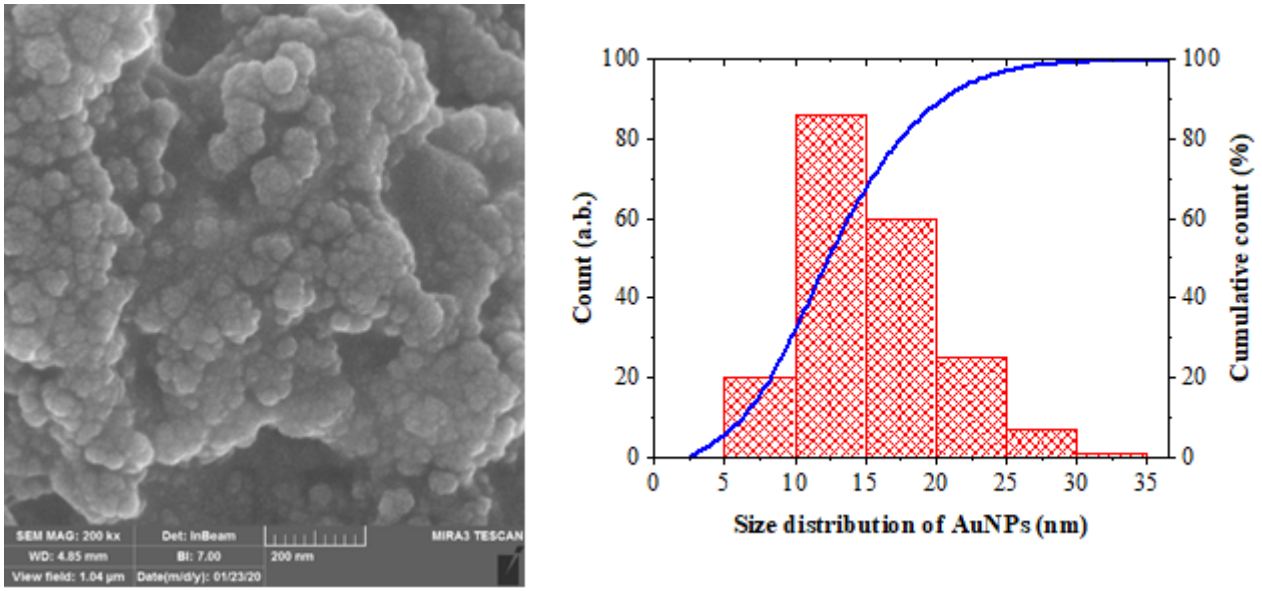

Figure 1

The FESEM image of colloidal Au nanoparticles and size distribution diagram of nanoparticles

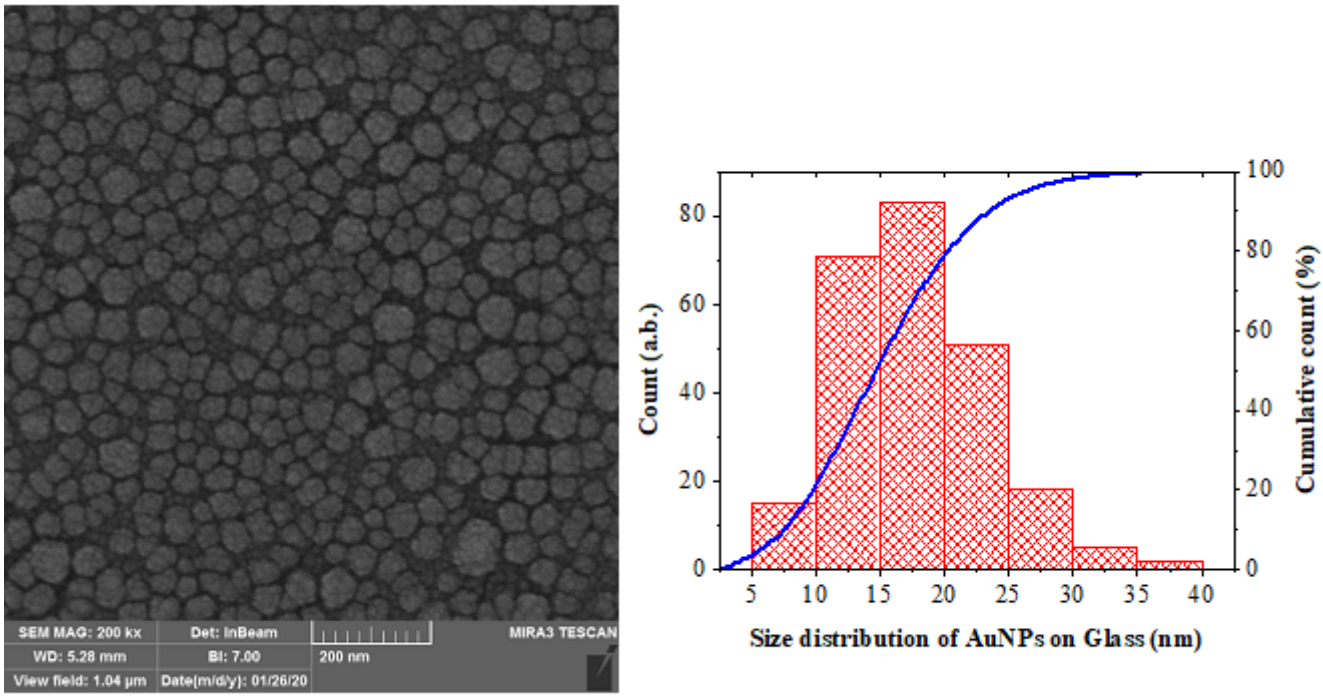

Figure 2

The FESEM image of Au nanoparticles on glass surface after annealing and size distribution diagram of nanoparticles

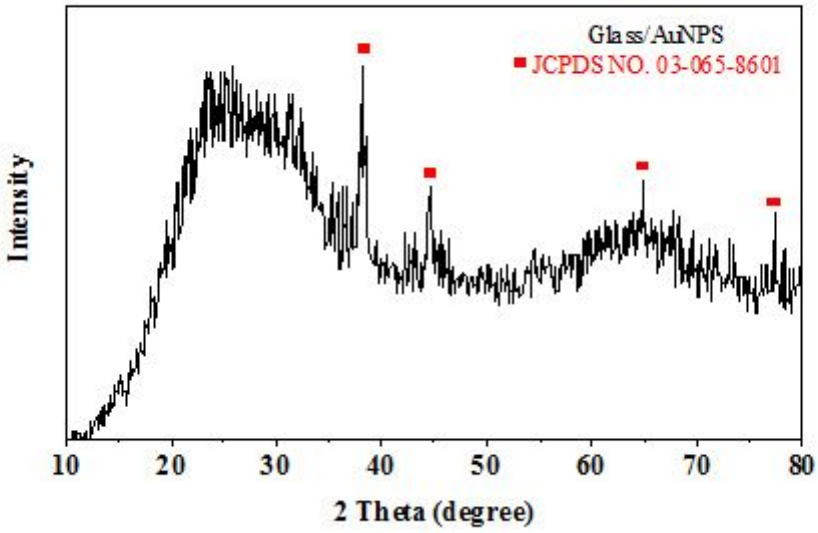

Figure 3

X-ray diffraction pattern of AuNPs thin film on glass substrate

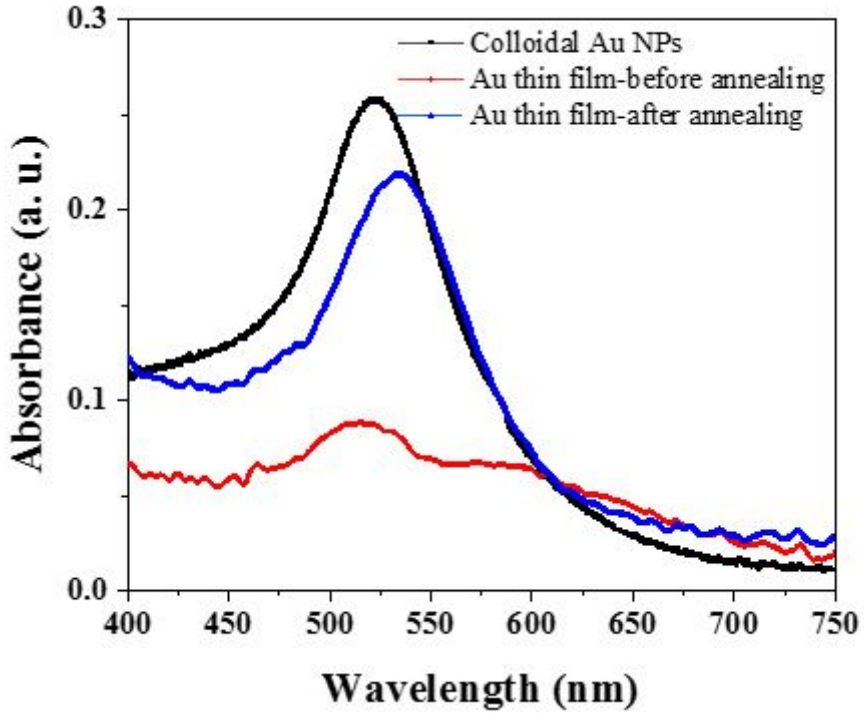

Figure 4

The absorbance of colloidal AuNPs, the LSPR sensor chips before and after annealing

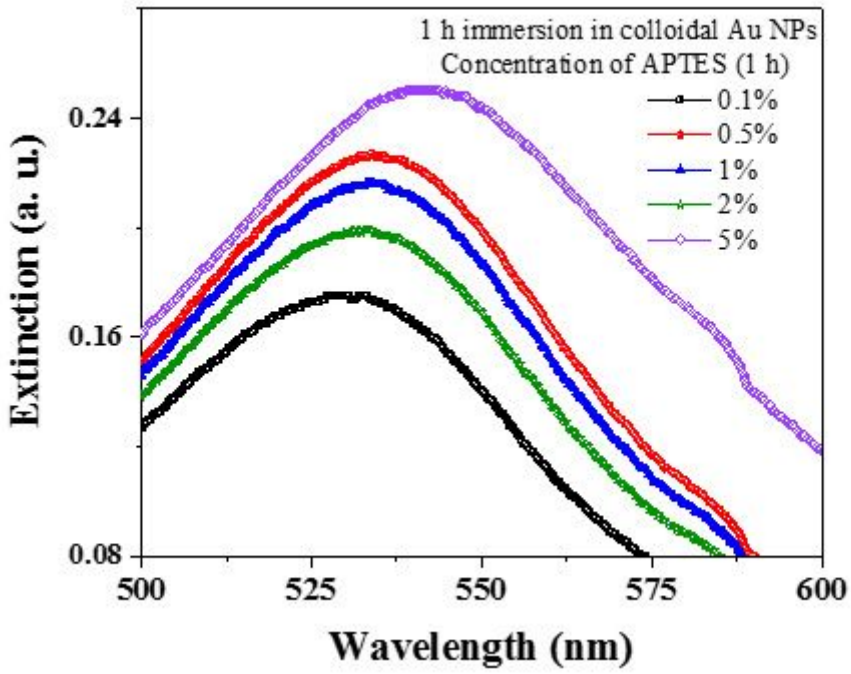

Figure 5

The extinction of LSPR sensor chip (type 1), 1 h in APTES with different concentration 0.1, 0.5, 1, 2, 5 % and 1 h immersion in colloidal AuNPs

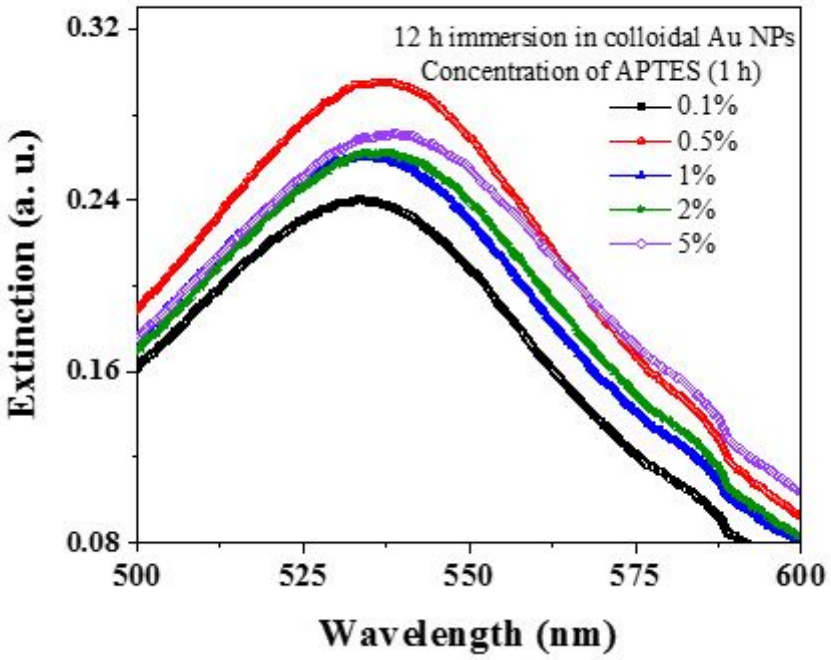

Figure 6

The extinction of LSPR sensor chip (type 2), 1 h in APTES with different concentration 0.1, 0.5, 1, 2, 5 % and 12 h immersion in colloidal AuNPs

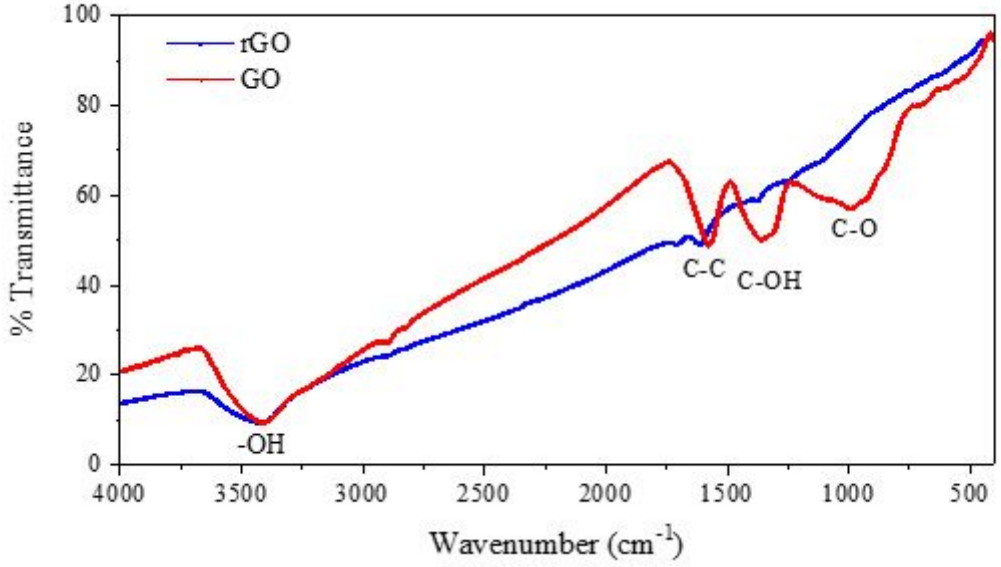

Figure 7

FT-IR spectra of GO and rGO sheets

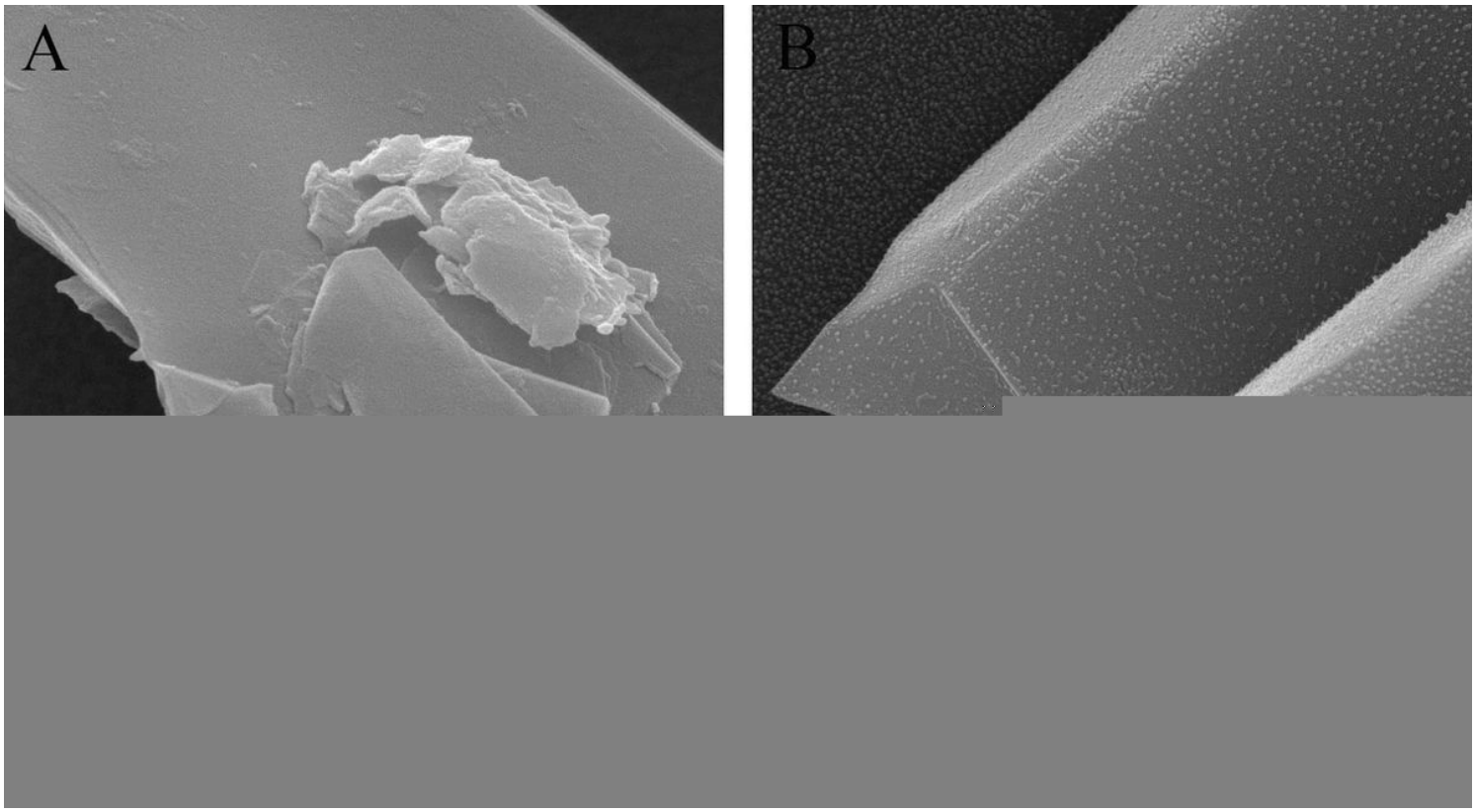

Figure 8

The FESEM image of LSPR chip of (a) AuNPs/rGO sheets and (b) AuNPs/GO sheets

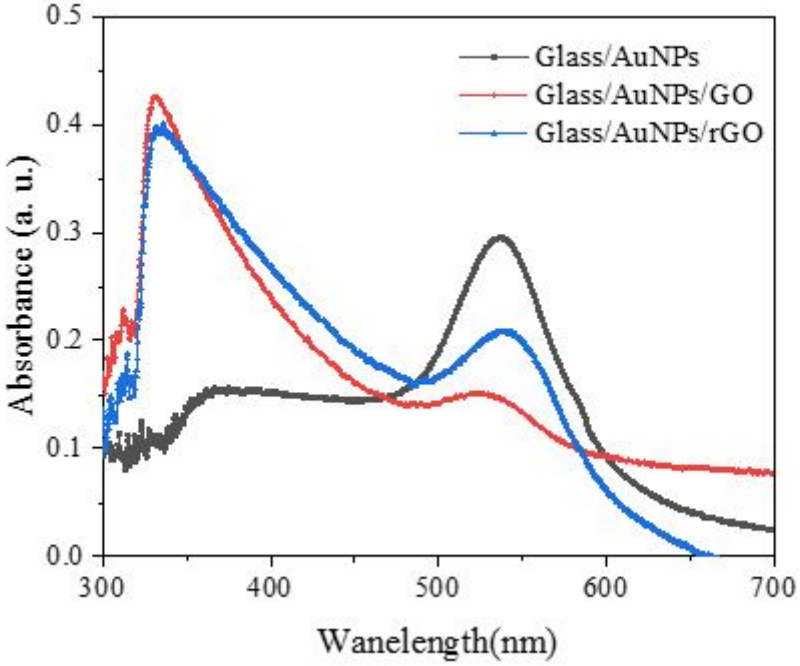

Figure 9

The absorbance spectra of Glass/ AuNPs and LSPR chip of AuNPs/GO sheets, LSPR chip of AuNPs/rGO sheets

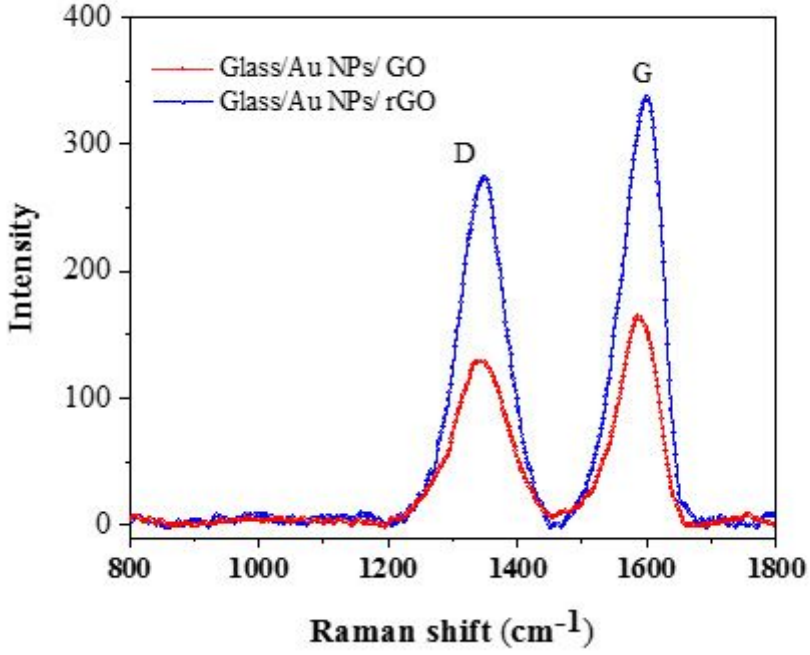

Figure 10

The Raman spectra of LSPR chip of AuNPs/GO sheets and LSPR chip of AuNPs/rGO sheets